Article

Influence of Highly Stable Ni^{2+} Species in Ni Phyllosilicate Catalysts on Selective Hydrogenation of Furfural to Furfuryl Alcohol

Sasithorn Kuhaudomlap, Okorn Mekasuwandumrong, Piyasan Praserthdam, Kiat Moon Lee, Christopher W. Jones,* and Joongjai Panpranot*

Read Online

ACCESS | Metrics & More | Article Recommendations | Supporting Information

ABSTRACT: Enhancing the catalytic performance of non-noble Ni catalysts in the selective hydrogenation of furfural to furfuryl alcohol (FA) in terms of furfural conversion, selectivity, and good recyclability is challenging. Here, spherical nickel phyllosilicate catalysts (Ni_PS) with fibrous-like structures are prepared via a modified sol−gel method with Ni loadings of 2−30 wt %. Upon exposure to air, all the reduced Ni_PS catalysts exhibit more than 80% Ni^0/Ni$_{phyllosilicate}$ species on the surface, whereas a large portion of Ni oxide species (>55%) is presented on the impregnated catalyst. The Ni^{2+} species in nickel phyllosilicate catalysts are active and highly stable during reduction, reaction, and regeneration, yielding stable catalytic performance for multiple recycle tests in furfural hydrogenation to FA. Furfural conversion over the Ni_PS catalysts increased monotonically with increasing Ni loading without an FA selectivity drop. The presence of both metallic Ni^0 and Ni$_{phyllosilicate}$ also produces a synergistic promotional effect for FA formation.

One-step modified spherical silica synthesis

INTRODUCTION

Nickel is one of the most frequently used metals in a wide variety of industrial manufacturing. Silica-supported nickel catalysts (Ni/SiO$_2$) are used extensively in catalytic reactions due to their low cost, high specific surface area, easy functionalization, and controllable morphology/adjustable pore structures.[1−3] However, Ni/SiO$_2$ usually suffers from a weak interaction between nickel species and silica supports, which is a significant drawback that can cause leaching of nickel species during a liquid phase reaction as well as agglomeration and sintering of nickel under a high thermal treatment and reaction process, leading to low catalytic activity, deactivation of catalyst, and poor stability. Several efficient strategies have been reported to improve nickel dispersion and enhance the metal−support interaction such as the addition of various promoters such as La$_2$O$_3$[4] and V$_2$O$_5$,[5] the formation perovskite and hydrotalcite structures,[6,7] the modification of the support and developed preparation methods to enhance the metal−support interaction and inhibit the catalyst agglomeration such as molecular layer deposition,[8] and the construction of nickel-based catalysts with a confinement effect like mesostructured cellular foam.[6] However, there are still some limitations for these methods such as high cost, complicated procedures, and requirement for multiple steps and unique instruments for preparation.

Metal phyllosilicates have received considerable attention in recent catalysis research because of their unique layered structure that can offer outstanding properties such as a strong metal−support interaction, small metal domain size and high dispersion of active metal species, rich porous structures, excellent adsorption properties, high thermal stability, and simple preparation procedures. Ni phyllosilicates typically possess a lamellar structure, consisting of tetrahedral layers of SiO$_4$ (Si-O-Si) and octahedral layers of Ni(II) (Ni coordinated to oxygen atoms or hydroxyl groups, Si-O-Ni-O(OH)).[9] It has been reported that metallic nickel derived from the reduction of nickel phyllosilicate can provide nickel particles with fine sizes at a high nickel content and high dispersion. Ni phyllosilicates show good performances in a number of reactions including CO$_2$ and CO methanation,[10] hydrogenation of levulinic acid to γ-valerolactone,[11] xylose hydrogenation to xylitol,[12] hydrogenation of maleic anhydride,[13] hydrogenation of polycyclic aromatic hydrocarbons,[14] and carbon dioxide reforming of methane.[15]

Generally, nickel phyllosilicates with different crystal structures can be synthesized via various methods including hydrothermal methods,[1,16−18] ammonia evaporation meth-
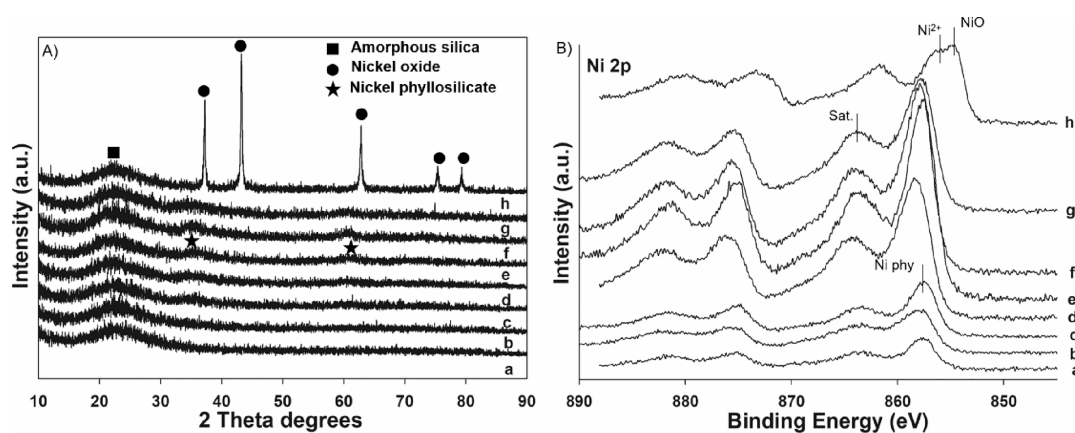
Figure 1. (A) XRD patterns and (B) Ni 2p XPS spectra of the calcined catalysts: (a) 2Ni_PS, (b) 5Ni_PS, (c) 10Ni_PS, (d) 15Ni_PS, (e) 20Ni_PS, (f) 25Ni_PS, (g) 30Ni_PS, and (h) 20Ni_Imp.

ods,[19−21] deposition−precipitation methods,[12,22] and sol−gel methods[23] through the reaction between a nickel precursor and silica materials. Among which, the hydrothermal method has been employed for preparation of nickel phyllosilicate catalysts due to high crystallinity, handy experimental operation, environmental friendliness, and uniform dispersion of nickel phyllosilicate. However, a conventional hydrothermal reaction is carried out in an autoclave under harsh hydrothermal conditions at high temperatures (>180 °C) with long reaction times (>24 h), resulting in the loss of the surface silanol group, limited nickel loading (even though there are excess nickel and silica amounts),[4,16,24,25] small amount of nickel phyllosilicate being formed, and large particles at relatively low hydrothermal temperatures (e.g., 120 and 160 °C).[10] Thus, it is a great challenge to improve and synthesize Ni phyllosilicates with high nickel contents under mild conditions and maintain the superior properties of nickel phyllosilicate. Chen et al.[18] synthesized nickel phyllosilicate with high nickel contents (22.4 wt %) using a urea-assisted hydrothermal method under a mild hydrothermal temperature and reaction time (180 °C, 24 h). The quick formation of nickel phyllosilicate was obtained because urea facilitates the formation of $Ni(OH)_2$ and leaching of SiO_2. Then, Chen and Liu[26] synthesized nickel phyllosilicate via the hydrothermal method assisted by NH_4F and urea, wherein the optimal nickel phyllosilicate (N/D-120-12) exhibited a high catalytic performance for CO_2 methanation and excellent anti-sintering properties. They reported that ammonium fluoride and urea can be an efficient accelerator of the formation of H_4SiO_4 and $Ni(OH)_2$, respectively, which are essential intermediates for the formation of nickel phyllosilicate. Nickel phyllosilicate could be formed under mild hydrothermal conditions at 100 °C for 12 h by double accelerators of ammonium fluoride and urea,[1] which has a similar morphology and nickel content with a conventional hydrothermal method at 220 °C for 48 h. Although this modified hydrothermal method can improve hydrothermal conditions, there are still some limitations of complicated operation procedures and too low hydrothermal conditions that provide a low nickel content and small amount of nickel phyllosilicate formation.[26]

Moreover, the preparation of nickel phyllosilicate usually consists of two major steps: step (1) is the silica material synthesis and step (2) is the nickel phyllosilicate formation via the reaction of a silica material and nickel precursor. It consumes large amounts of reagent and energy and requires a long operation time. One-pot synthesis of Ni phyllosilicates has recently been reported, for example, Chen et al.[24] prepared 3D-SBA-15-derived Ni phyllosilicate via a one-pot and two-pot hydrothermal methods at 180 °C. One-pot synthesis exhibited small size nickel particles and showed high anti-sintering due to a strong metal−support interaction derived from nickel phyllosilicate. Many advantages of one-pot synthesized nickel phyllosilicate catalyst (Ni/S-O) were achieved including low cost, monolithic appearance, fine nickel particle size, high nickel phyllosilicate content, high convenience, and elimination of the separation, drying, and calcination process. In addition, it was found that hydrothermal conditions were significant for the formation of nickel phyllosilicate via one-pot synthesis, in which sectional hydrothermal treatment at 100 °C for 24 h and 180 °C for 24 h affected the formation of nickel phyllosilicate in their work.

In this study, spherical silica-derived nickel phyllosilicate (Ni_PS) was successfully prepared via one-step modified spherical silica synthesis with alternate addition of nickel and silica precursor under room temperature. The one-step synthesized Ni_PS catalysts with various nickel loadings (2−30 wt % Ni) were characterized by H_2-TPR, STEM, EDS, and XPS, and their catalytic properties were evaluated in the liquid-phase selective hydrogenation of furfural to furfuryl alcohol (FA) under mild reaction conditions in order to simultaneously obtain an excellent anti-leaching property and improve the catalytic activity. Furfural, synthesized via catalytic dehydration of xylose in hemicellulose, is a versatile platform molecule that can be further converted into many high value derivatives and downstream fine chemicals and biofuels. Among the non-noble metal catalysts for furfural hydrogenation, Ni has been demonstrated to be a good furfural hydrogenation catalyst due to its excellent H_2 dissociation and relatively low cost.

■ RESULTS AND DISCUSSION

Characterization of the Calcined Catalysts. The presence of nickel phyllosilicate and nickel oxide on the prepared catalysts was probed by XRD, and the results are shown in Figure 1. A broad peak located at $2\theta = 23°$, which is a characteristic peak of amorphous oxide, was observed for all the samples. The catalysts prepared by one-step modified spherical silica synthesis display major diffraction peaks at 2θ degrees = 34.1 and 60.8, which are attributed to the nickel phyllosilicate structure.[15] The intensity of the characteristic
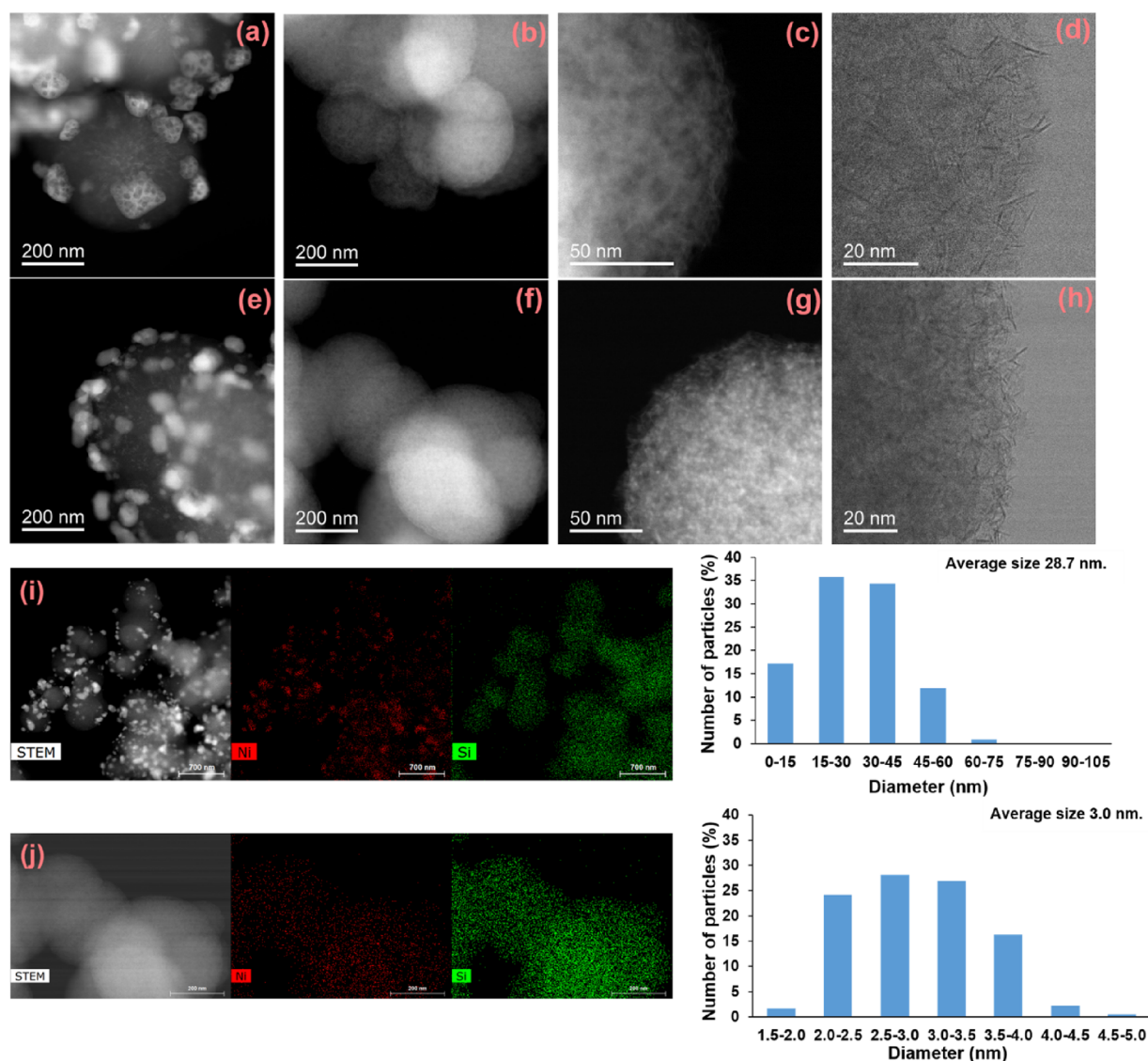
Figure 2. TEM images of the nickel catalysts: (a) calcined-20Ni_Imp, (b−d) calcined-20Ni_PS, (e) reduced-20Ni_Imp, and (f−h) reduced-20Ni_PS. EDS mapping images and the Ni particle size distribution histogram of (i) reduced-20Ni_Imp and (j) reduced-20Ni_PS.

diffraction peaks of nickel phyllosilicate increased with increasing nickel loading from 10 to 30 wt % and was not observed with low nickel loading (2−5 wt %), which may be due to a small amount/low crystallinity of nickel phyllosilicate (Figure 1A). On the other hand, the sharp diffraction peaks assigned to nickel oxides were clearly evident as expected at 2θ = 37.3, 43.3, 62.8, 75.5, and 79.3°[27] in the XRD patterns of the 20Ni_Imp catalyst. The oxidation states of nickel species on the catalyst surface before reduction/passivation were analyzed by XPS, and the results are shown in Figure 1. As shown in Figure 1B, the Ni $2p_{3/2}$ peaks of the calcined 20Ni_Imp were deconvoluted into two peaks at binding energies 854.2 and 856.2 eV, which were assigned to aggregated NiO and highly dispersed Ni^{2+}, respectively.[21,28] For all the calcined Ni_PS catalysts, the observed strong peaks at around 857−859 eV were assigned to Ni^{2+} species that strongly interact with silica in the nickel phyllosilicate structure.[15] The XPS peak intensity can be used to indicate the different levels of nickel dispersed on the catalyst surface.[29] The results demonstrate that the nickel phyllosilicate phase was successfully obtained by one-step modified spherical silica synthesis even for a relatively low

nickel content (2 wt %) under mild conditions (room temperature and a short time).

The structures and morphologies of the calcined catalysts are shown in the TEM images in Figure 2. All the prepared catalysts displayed a spherical particle shape, with average size ca. 0.30 μm for the series of Ni_PS samples. The average particle size was slightly decreased with increasing nickel loading (∼0.2 μm for 30Ni_PS) and was ca. 0.5 μm for the 20Ni_Imp catalyst. Owing to the simultaneous loading of nickel and silica precursors during one-step modified spherical silica synthesis, nickel can form within the structure and on the surface, and nickel densities were increased from the unique structure of nickel phyllosilicate that interfere with each other, resulting in a smaller particle size with increasing nickel loading. According to the literature, the decrease in the particle size of mesostructured silica nanoparticles (MSN) resulted in the improved formation of nickel phyllosilicate due to the increase in surface silanol group concentration.[30] A fibrous-like structure was observed on the nickel phyllosilicate catalysts, whereas on the impregnated catalysts, large metal oxide particles (d_p ∼ 60 nm) were formed on the spherical silica

support. It is confirmed that nickel phyllosilicate was successfully formed under relatively mild conditions. The N_2 physisorption results and the corresponding nitrogen adsorption−desorption isotherms are shown in Table 1 and Figure

Table 1. Physical Properties of the Calcined Catalysts and CO Pulse Chemisorption Results

catalysts	BET surface area (m^2/g)	pore volume (cm^3/g)	pore diameter (nm)	CO adsorption $(\mu mol/g_{cat})^a$
SSP	1084	0.79	2.6	
2Ni_PS	977	0.77	2.9	10.3
5Ni_PS	491	0.47	3.5	10.4
10Ni_PS	168	0.06	3.8	9.8
15Ni_PS	185	0.11	4.2	10.8
20Ni_PS	234	0.19	4.0	37.6^b
				35.8
25Ni_PS	219	0.20	4.9	26.5
30Ni_PS	260	0.15	4.4	19.3
20Ni_Imp	828	0.55	2.5	1.9^b
				11.4

^{a}Determined by CO-pulse chemisorption: catalysts were reduced at 500 °C for 3 h. ^{b}Calcined catalysts.

S1. The specific surface area, pore volume, and pore size diameter of the bare spherical silica support are 1084 m^2/g, 0.79 cm^3/g, and 2.6 nm, respectively. Compared to the bare SiO_2, all the Ni_PS catalysts with 2−30 wt % Ni loading possessed lower BET surface areas and smaller pore volumes with slightly larger average pore diameters. The BET surface area and pore volume decreased from 977 to 168 m^2/g and 0.77 to 0.06 cm^3/g with an increasing Ni loading from 2 wt % to 10 wt % and then slightly increased to reach a 260 m^2/g surface area and 0.15 cm^3/g pore volume for the 30Ni_PS sample. Typically, the formation of the fibrous-like structure of nickel phyllosilicates can result in an increased specific surface area and pore volume, compared to the silica support and impregnation-based catalysts.[9,13,31] This correlates with a unique porous structure for the lamellar nickel phyllosilicate. However, a different trend was observed in the present work. Here, nickel phyllosilicate was formed by simultaneous loading of nickel and silica precursors during the one-step modified spherical silica synthesis with CTAB as the structure directing agent followed by calcination at 550 °C for 6 h. For Ni loadings ≤10 wt % on the spherical silica, the higher surface area could be attributed to the mesostructured SiO_2 being formed in addition to the nickel phyllosilicate phase, as confirmed by the presence of mesopores in the adsorption isotherm. Samples with larger nickel loadings lacked mesopores according to the nitrogen physisorption isotherms. Further increases in Ni loading to 15, 20, 25, and 30 wt % led to an increase in BET surface area as a result of the formation of fibrous-like structure of the nickel phyllosilicate domains. The specific surface area and pore volume of the 20Ni_Imp catalyst were 828 m^2/g and 0.55 cm^3/g, respectively, which were comparable to those of the Ni_PS samples with Ni loadings between 2 and 5 wt %.

The reducibility of both Ni_PS and 20Ni_Imp catalysts was further investigated by H_2-TPR, and the results are shown in Figure 3. The impregnation catalyst exhibited two reduction peaks, a strong reduction peak at 342 °C and a weak shoulder peak at around 489 °C, which are attributed to the reduction of the nickel oxide species and the weak interaction between
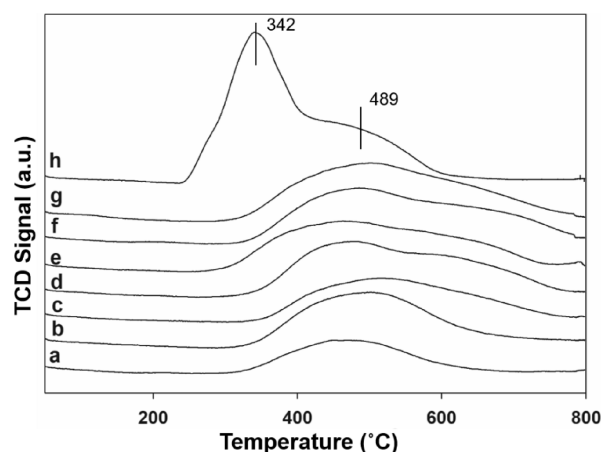

Figure 3. H_2-TPR profiles of the calcined catalysts: (a) 2Ni_PS, (b) 5Ni_PS, (c) 10Ni_PS, (d) 15Ni_PS, (e) 20Ni_PS, (f) 25Ni_PS, (g) 30Ni_PS, and (h) 20Ni_Imp.

isolated nickel ions (Ni^{2+}) and SiO_2, respectively.[21] Interestingly, all the Ni_PS catalysts exhibited only broad reduction peaks in the high temperature ranges from 500 to 800 °C, which are assigned to the reduction of Ni^{2+} located in the nickel phyllosilicate with strong interaction between nickel species and silica.[21] These nickel species existed mostly in the form of strong, chemically bonded Ni-O-Si species in the nickel phyllosilicate structure. Additionally, the reduction peak tended to shift to a higher temperature and larger area with increasing nickel loading from 2 to 30 wt %, indicating a higher amount of nickel phyllosilicate and a more difficult reduction. The H_2-TPR results suggest the incomplete reduction of nickel species to metallic metal for all catalysts during the reduction process at 500 °C for 3 h prior to the reaction tests.

Characterization of the Reduced Catalysts. After reduction with H_2 at 500 °C for 3 h (Figure 4), the distinct
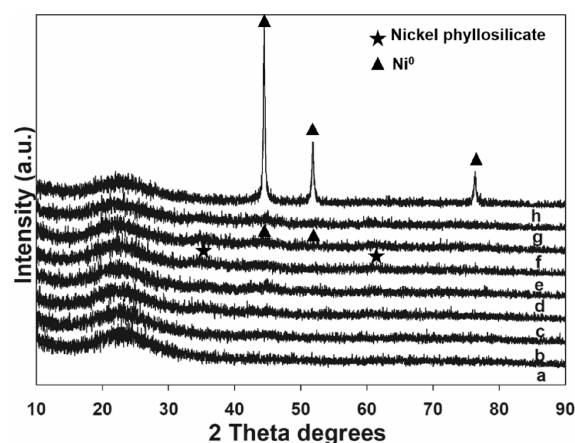

Figure 4. XRD patterns of the reduced catalysts (a) 2Ni_PS, (b) 5Ni_PS, (c) 10Ni_PS, (d) 15Ni_PS, (e) 20Ni_PS, (f) 25Ni_PS, (g) 30Ni_PS, and (h) 20Ni_Imp.

XRD peaks at 2θ = 44.6, 51.8, and 76.2° observed on 20Ni_Imp are ascribed to metallic nickel,[32] indicating that the crystalline nickel oxides on the impregnation catalyst were primarily reduced to nickel metal. On the series of reduced/passivated Ni_PS catalysts, the diffraction peaks of nickel phyllosilicate were moderately weakened and disappeared for Ni_PS with nickel loadings ≤10 wt %. Small diffraction peaks
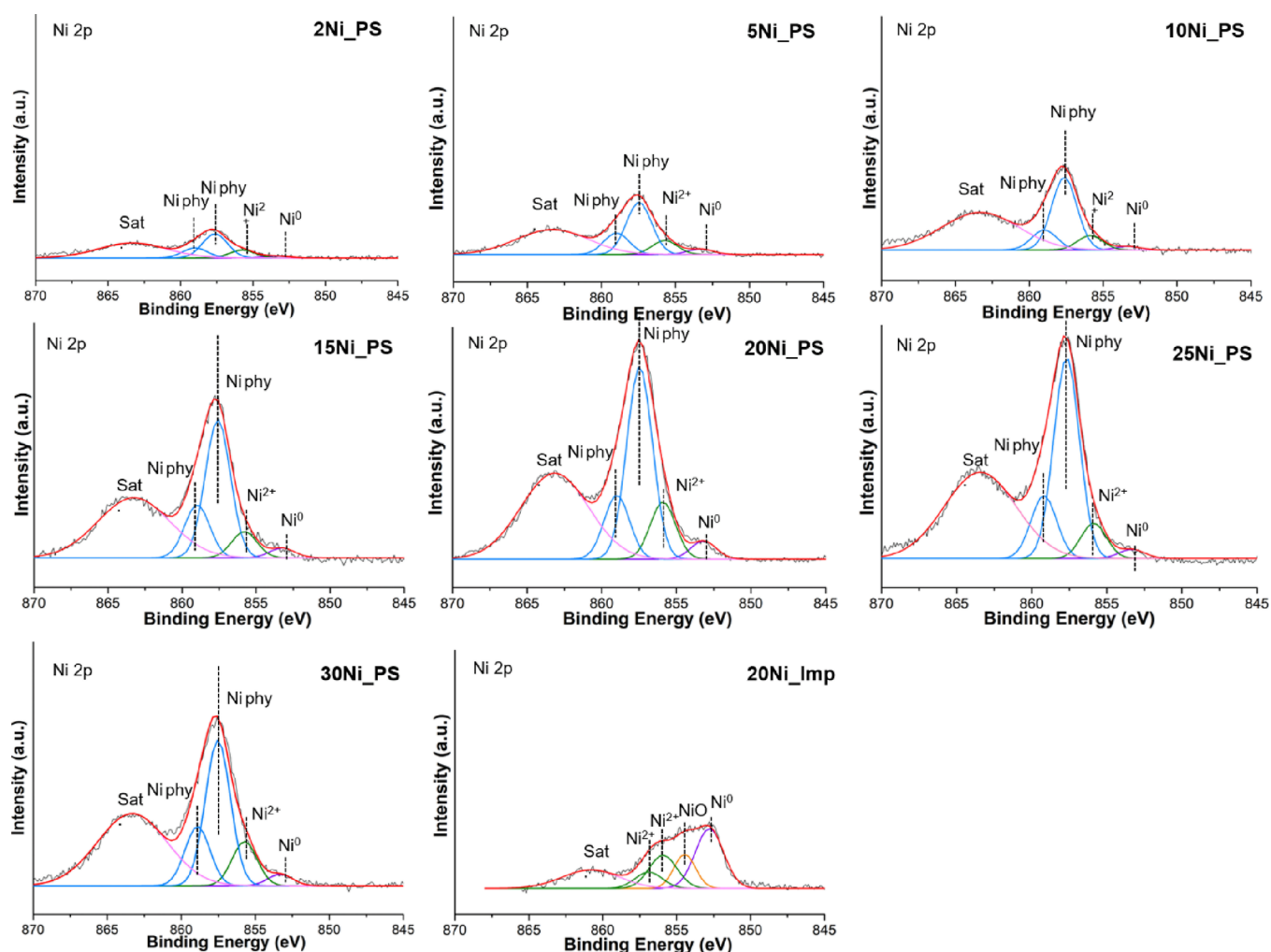
Figure 5. Ni 2p XPS spectra of the reduced/passivated catalysts.

corresponding to metallic nickel were additionally detected on the reduced Ni_PS with relatively high Ni loadings (e.g., ≥15 wt % Ni). Such results indicate the co-existence of nickel phyllosilicate and nickel metal on the reduced Ni_PS, whereas the crystalline nickel oxide species appeared totally reduced into metallic nickel on 20Ni_Imp. In addition, the morphologies of the reduced/passivated catalysts are shown in the TEM images in Figure 2 along with the elemental mapping of Ni and Si species on the catalysts. Small bright spots representing nickel metal domains were well distributed on both types of reduced samples. As shown in Figure 2f−h, high dispersion of small nickel particles on the catalyst surface without any large aggregation was observed over 20Ni_PS, in addition to the fibrous-like structure of the nickel phyllosilicate, which remained after reduction. The TEM results are consistent with the XRD and H_2-TPR results, showing that the nickel phyllosilicate species were not completely reduced under the reduction conditions used in this work. The average diameters of the nickel particles on the reduced catalysts as well as their size distribution histograms are shown in Figure 2j,i,. The average nickel particles after reduction at 500 °C for the reduced 20Ni_PS and 20Ni_Imp are 3 and 29 nm, respectively. It can be implied that the remaining nickel phyllosilicate layer after the reduction process act as the support on metallic nickel, which resulted in the highly dispersed and homogeneous nickel particles with small sizes at

high loading.[31] The nickel phyllosilicate catalyst is highly resistant to sintering and is highly stable because of the enhanced interaction of Ni and SiO_2 in the nickel phyllosilicate layers, preventing agglomeration under high temperature reduction processes such as the method deployed here.[15,16,21]

The Ni 2p XPS spectra of the reduced/passivated catalysts were deconvoluted into five peaks, as shown in Figure 5. The first peak at 853.3 eV is assigned to Ni^0 species. The binding energy at 855.8 eV belongs to the highly dispersed Ni^{2+}, and the strong peaks at around 857.6 and 859.0 eV were ascribed to Ni^{2+} species with strong interactions with SiO_2 in the nickel phyllosilicate structure. The last peak centered at 862 eV is attributed to the Ni 2p satellite peak due to electron shake-up.[13] As also revealed by H_2-TPR results, the nickel phyllosilicate species could not be totally reduced at 500 °C, and thus, the XPS peaks corresponding to nickel phyllosilicate domains were still apparent on the catalysts after reduction/ passivation. For the reduced/passivated 20Ni_Imp, the Ni $2p_{3/2}$ peaks were deconvoluted into three typical nickel species at binding energies of 852.8, 854.5, and 855.9−856.9 eV, which correspond to metallic nickel Ni^0, NiO, and highly dispersed Ni^{2+}, respectively.[4,21] Compared to the metallic Ni^0 peaks of 20Ni_Imp at 852.8 eV, the Ni^0 peaks of the Ni_PS catalyst were shifted to a higher binding energy at 853.3 eV, indicating a stronger interaction between nickel metal and the silica support of the nickel phyllosilicate catalysts. Such results

are in good agreement to the well-established trend in the literature.[33] The surface atomic ratios of $Ni_{(total)}$/Si, Ni^0/Si, (NiO + Ni^{2+})/Si, and $Ni_{Phyllosilicate}$/Si of various catalysts are provided in Table 2. The surface atomic ratios of $Ni_{(total)}$/Si on the Ni_PS catalysts increased with increasing Ni loading and appeared to reach a threshold limit at around 20−25 wt % Ni. For a similar Ni loading (20 wt % Ni), the surface atomic ratio of Ni^0/Si on the reduced/passivated 20Ni_PS catalysts is lower compared to the reduced/passivated impregnation catalyst (20Ni_Imp), which is consistent with the H_2-TPR results, showing that the impregnation catalyst was easier to reduce than the nickel phyllosilicate materials. However, the surface atomic ratios of $Ni_{(total)}$/Si on 20Ni_PS was twice that of 20Ni_Imp, indicating a large amount of Ni phyllosilicate species on the catalyst surface. Moreover, the surface atomic ratios of Ni^0 + $Ni_{phyllosilicate}$/Ni_{total} and the ratio of Ni^{2+}+NiO/ Ni_{total} species were calculated and are shown in Table 2. These percentages showed the relative coverages of different nickel species on the catalyst surface. All the reduced Ni_PS catalysts exhibit more than 80% Ni^0 + $Ni_{phyllosilicate}$/Ni_{total} species on the surface, whereas a large portion of Ni^{2+} and Ni oxide species (>55%) was present on the impregnated catalyst after reduction. The presence of Ni^{2+} and NiO on the reduced catalysts could be due to the re-oxidization of metallic nickel upon exposure to air during sample transfer. Nevertheless, the Ni_PS catalysts exhibited a stable nickel phyllosilicate species on the surface. CO pulse chemisorption was performed to evaluate the number of potential Ni active sites on the catalysts, assuming that one CO molecule adsorbed on one nickel site, and the results are reported in Table 1. On the calcined catalysts, the amounts of CO adsorbed on the calcined 20Ni_Imp and 20Ni_PS were 1.8 and 37.6 μmol/g, respectively. It is suggested that CO cannot adsorb on bulk nickel oxides but can adsorb on nickel phyllosilicate domains. The amounts of CO adsorbed on the reduced catalysts are as follows: 2Ni_PS (10.3 μmol/g), 5Ni_PS (10.4 μmol/g), 10Ni_PS (9.8 μmol/g), 15Ni_PS (10.8 μmol/g), 20Ni_PS (35.8 μmol/g), 25Ni_PS (26.5 μmol/g), and 30Ni_PS (19.3 μmol/g). The amounts of CO adsorbed on the Ni_PS catalysts with 2−15 wt % Ni were quite similar, being around 10 μmol/ g. The amount of CO adsorbed was maximized on the 20 wt % nickel loading, the 20Ni_PS catalyst, at 35.8 μmol/g, which was much higher than 20Ni_Imp (11.38 μmol/g). A further increase in Ni loading to 25 and 30 wt % resulted in a decline of adsorbed CO to around 20 μmol/g. Nevertheless, the results suggest that both metallic Ni^0 and Ni^{2+} in the phyllosilicate structure were active for CO chemisorption and may provide high active sites for a furfural hydrogenation reaction. In a recent study by Meng et al.,[34] CO-IR was carried out on Ni supported on mixed metal oxides that were prepared via structural topological transformation from hydrotalcites (LDHs) precursors with nitrate in the interlayer region (Ni/ MMO-NO_3). The in situ CO-IR confirmed a large proportion of steps/edges of Ni nanoparticles in these catalysts, which facilitates adsorption of the C=O group. It is believed that the high CO chemisorption ability of Ni phyllosilicate catalysts is also due to the presence of a large amount of edge sites. It has previously been suggested that Ni phyllosilicate is composed of fragments of the same layer-like structure, which has large proportions of edges.[34] Moreover, the coordinatively unsaturated Ni(II) sites near the edges/surfaces of phyllosilicate are Lewis acid sites.

Table 2. Ni Peak Fitting Parameters and Ni Species Proportion over the Surface of Reduced/Passivated Catalysts in Ni 2p

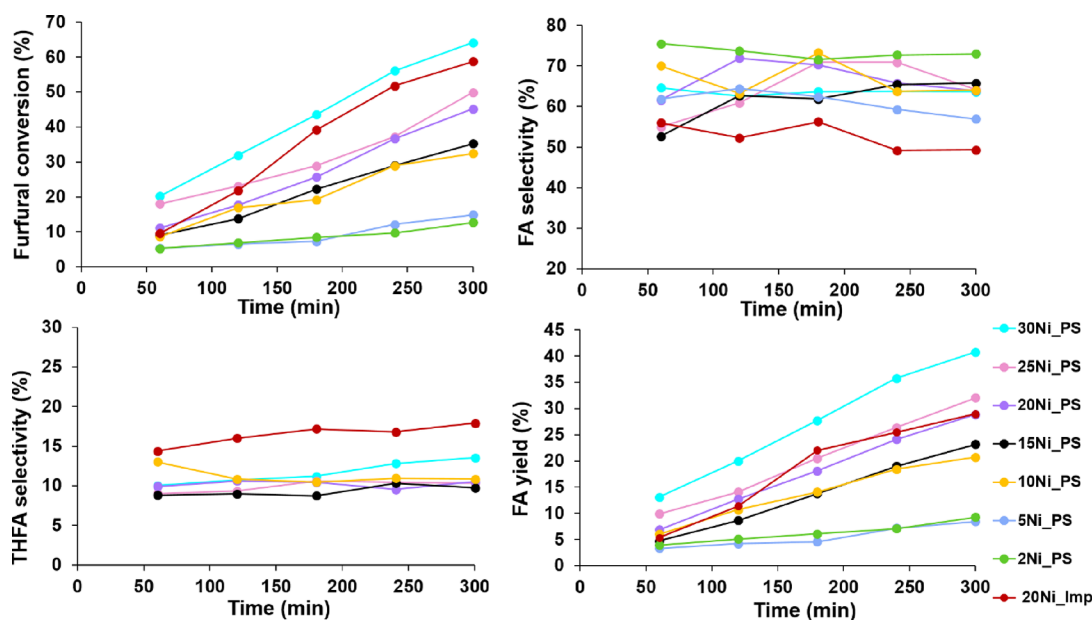| catalysts	Ni^0 B.E. (eV)	Ni^0 FWHM	NiO B.E. (eV)	NiO FWHM	Ni^{2+} highly dispersed B.E. (eV)	Ni^{2+} highly dispersed FWHM	Ni phyllosilicate B.E. (eV)	Ni phyllosilicate FWHM	atomic surface ratio Ni/Si	Ni^0/Si	NiO + Ni^{2+}/Si	Ni phy/Si	Ni^0 + Ni_{phy}/Ni (%)	TOF (h^{-1})
2Ni_PS	853.4	1.98			855.7	1.98	857.6 / 859.0	2.02 / 1.98	1.15	0.05	0.21	0.89	81.7	60.01
5Ni_PS	853.3	1.98			855.7	1.99	857.5 / 859.0	2.02 / 1.99	2.12	0.12	0.32	1.68	84.9	62.84
10Ni_PS	853.3	1.99			855.9	2.00	857.6 / 859.0	2.01 / 2.00	2.30	0.07	0.30	1.93	87.0	103.93
15Ni_PS	853.2	2.01			855.9	2.00	857.6 / 859.0	2.01 / 1.98	7.06	0.30	0.81	5.94	88.4	100.80
20Ni_PS	853.2	1.98			855.9	1.99	857.5 / 859.0	2.03 / 1.99	9.50	0.51	1.61	7.37	82.9	37.00
25Ni_PS	853.3	2.02			855.9	1.99	857.7 / 859.2	2.01 / 2.01	9.89	0.30	1.12	8.47	88.7	80.69
30Ni_PS	853.3	1.98			855.7	1.98	857.5 / 858.9	1.99 / 1.98	8.11	0.36	1.37	6.38	83.1	124.35
20Ni_Imp	852.8	2.25	854.5	1.71	855.9 / 856.9	2.22 / 2.16			4.78	2.14	2.65	0.00	55.0 (NiO + Ni^{2+}/Ni)	100.29

Figure 6. Hydrogenation of furfural to FA over nickel phyllosilicate catalysts with varying nickel loading and impregnation catalyst (20Ni_Imp) versus reaction time. Reaction conditions: 250 mg of catalyst, 3 mmol of furfural, 50 mL of methanol solvent, 0.4 mmol of dodecane, reaction temperature of 50 °C, 20 bar H_2 pressure, reaction time of 5 h, and catalysts were reduced at 500 °C.

Catalytic Test Results. The catalytic performances of the prepared catalysts were evaluated in the selective hydrogenation of furfural to FA at 50 °C under a H_2 pressure of 20 bar for 5 h with methanol as the solvent. All the catalysts were reduced at 500 °C under a H_2 flow for 3 h and passivated prior to the reactions. Furfural is an interesting biomass platform molecule that contains several functional groups in its structure, which can be hydrogenated to various products. The desired product in this work is FA, while THFA was found as a minor product. The blank test result is shown in Table S1; 2-furaldehyde dimethyl acetal was the only byproduct obtained (~6% conversion), which was produced by the solvent reaction via an acetalization mechanism.[35,36] The influences of nickel loadings in the range of 2−30 wt % Ni in the Ni_PS catalysts on furfural conversion, selectivity, and FA yield as a function of reaction time are shown in Figure 6.

Typically, furfural conversion and FA selectivity over nickel catalysts increase with increasing nickel loading up to an optimum amount (e.g., 4.6%Ni in the Ni-Cu/ZrO_2 catalyst[37] and 10%Ni/CNT[38]) and then decrease with further increases of nickel content, which is possibly due to agglomeration of Ni particles at high Ni loadings, resulting in low metal dispersion/low activity.[7] Interestingly, furfural conversion of all the Ni_PS catalysts monotonically increased with increasing nickel loading from 2 to 30 wt % Ni. Although the CO chemisorption and XPS results suggest the largest availability of active sites and the highest Ni^0/Si on the surface at 20 wt % Ni loading, furfural conversion continued to increase on 30Ni_PS compared to 20Ni_PS and 25Ni_PS. For a similar Ni loading at 20 wt %, 20Ni_Imp exhibited a higher hydrogenation rate than 20Ni_PS. The furfural conversion values over 20Ni_Imp and 20Ni_PS after 5 h of reaction time were 58 and 48%, respectively. However, it can be clearly seen that all the nickel phyllosilicate catalysts exhibited a higher FA selectivity (65−75%) than 20Ni_Imp (~48% FA). The selectivity of THFA on all the Ni_PS catalysts was below 10% (except for 30Ni_PS, where the THFA selectivity was ~13%), while that of

20Ni_Imp was >15%. According to the literature and as shown in Figure 6, the selectivity of FA and THFA did not depend on furfural conversion and reaction time and was rather affected by the electronic properties of Ni species and/or Ni−support interaction.[34,39−42]

A proposed reaction pathway for furfural hydrogenation over Ni-based catalysts is shown in Figure S2. Hydrogenation of the carbonyl group (C═O) in furfural produces the desired product FA, and further hydrogenation of FA (C═C) results in THFA. Other byproducts such as furan, tetrahydrofuran, methyl furan, etc. are produced in a small amount (total selectivity ≤10%). The carbon balances (Table S1) were calculated above 85% over all samples for each time point. Typically, supported Ni catalysts without modification/addition of a promoter produce a higher selectivity toward THFA than FA (76−91% selectivity of THFA).[38,43] The use of high surface area spherical silica in this study can enhance the FA selectivity of the impregnated Ni/SiO_2 catalysts since significant amounts of highly dispersed Ni^{2+} species were formed on the 20Ni_Imp catalyst, as revealed by the XPS results. Based on the catalyst characterization and reaction results, nickel phyllosilicate species were active for both CO chemisorption and also for furfural hydrogenation under mild reaction conditions. The synergistic effect of highly dispersed nickel particles and Lewis acid sites of the remaining nickel phyllosilicate contributes to the low-temperature hydrogenolysis/hydrogenation in biomass conversion.[9,31] For the same Ni loading (20 wt % Ni), the amount of CO adsorbed on 20Ni_PS was much higher than 20Ni_Imp, despite its lower hydrogenation activity. The larger amounts of CO chemisorption on the Ni_PS catalysts were correlated to the larger amounts of Ni phyllosilicate being formed, and not the higher hydrogenation activity. In other words, Ni_PS exhibited a higher CO chemisorption ability but the hydrogenation activity of Ni phyllosilicate species was lower than metallic Ni^0. It is widely accepted that metallic Ni^0 species function as active sites for H_2 dissociation[13,14,44] while Ni^{2+} in NiO is
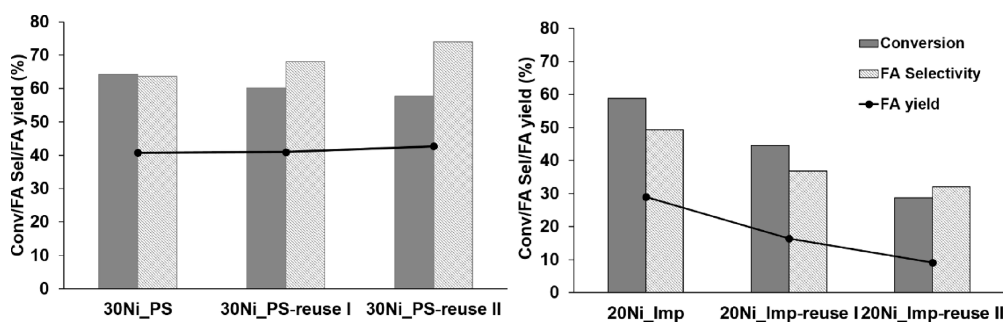
Figure 7. Recycle test for the hydrogenation of furfural to FA over 30Ni_PS and 20Ni_Imp catalysts with three repeated runs. Reaction conditions: 250 mg of catalyst, 3 mmol of furfural, 50 mL of methanol solvent, 0.4 mmol of dodecane, reaction temperature of 50 °C, 20 bar H_2 pressure, reaction time of 5 h, and catalysts were reduced at 500 °C.

inactive. However, Ni^{2+} species that strongly interact with SiO_2 can play an important role in binding and activating the C=O group in the furfural structure, as suggested by CO chemisorption results. The high CO chemisorption ability suggests their high ability to facilitate activated adsorption of the C=O group in furfural hydrogenation to furfuryl alcohol. According to the literature, Ni phyllosilicate, which is composed of fragments of layer-like structures with large proportions of edges, is therefore active and selective for the activation of the C=O group, resulting in high selectivity toward furfuryl alcohol.[31,34] It was reported that the adsorption configuration of substrate plays a key role in determining the hydrogenation pathway and selectivity. The existence of specific active sites on the catalyst surface would induce unique adsorption configuration of substrate, which imposes an essential impact on the hydrogenation pathway and product selectivity.[34] The electron-deficiency of some Ni^{2+} atoms may allow them to act as Lewis acid sites for the adsorption of the C=O bond through oxygen atoms, which likely enhances the adsorption and conversion of furfural.[45] The presence of both metallic Ni^0 and highly dispersed Ni^{2+} that strongly interact with SiO_2 is suggested to be necessary for high furfural conversion and high FA selectivity under mild reaction conditions.

The turnover frequency (TOF) based on the moles of furfural converted and the number of active sites measured by CO-chemisorption per hour has now been reported. Compared to the other Ni-based catalysts reported in the other literature, Ni_PS catalysts showed relatively high TOF values with a maximum TOF of 124.35 h^{-1} for the 30Ni_PS catalyst and demonstrated a high catalytic performance under mild conditions among the various studies (low reaction temperature and H_2 pressure), as indicated in Table S2. There was no significant difference in the TOF value for all Ni loadings since the TOF value did not depend on Ni^{2+} species at a high nickel loading and was rather correlated to the surface proportion of active species and average particle size.[46,47] A loading of 20 wt % Ni by impregnation on high surface area spherical silica resulted in about 50:50 metallic Ni^0 species: (NiO/highly dispersed Ni^{2+}), as revealed by XPS results. As a result, the 20Ni_Imp catalyst exhibited a relatively high conversion of furfural but the selectivity of FA was the lowest among the catalysts studied, producing the highest %THFA. 20Ni_PS (78% Ni phyllosilicate species, 5% Ni^0) showed a lower activity and TOF value with a higher FA selectivity, and as a consequence, the FA yield was essentially similar to that of 20Ni_Imp ($\sim$50%Ni^0). This is because the hydrogenation activity of Ni phyllosilicate is lower than metallic Ni^0.

However, increasing the Ni loading on Ni_PS to 30 wt % can further increase the furfural conversion without any change in FA selectivity, resulting in a much higher FA yield on 30Ni_PS.

Catalyst Recyclability Tests. The recyclability of the catalysts was investigated on the 30Ni_PS and 20Ni_Imp catalysts by conducting a three cycle run under identical conditions at 50 °C under 20 bar H_2 pressure for 5 h. After use, the spent catalysts were washed with methanol solvent several times and were subjected to H_2 reduction at 500 °C for 3 h before being reused for furfural hydrogenation. The recyclability results are shown in Figure 7. It is clear that 30Ni_PS exhibited an excellent recyclability for furfural hydrogenation with enhanced FA selectivity. The conversion decreased slightly (by $\sim$10%), while the FA selectivity increased from 64 to 74% in the third cycle. On the other hand, the 20Ni/_Imp catalyst showed poor reusability. Furfural conversion drastically declined from 58% for the fresh catalyst to 29% in the third cycle ($\sim$50% change) with a significant drop of FA selectivity from 48 to 32% in the third run.

The spent catalysts after three runs were further characterized by TEM and XPS to examine the changes in the characteristics of the catalysts after reaction, and the results are shown in Figure S3, Figure S4, and Table S3. TEM images confirm that there were no significant changes in the morphology of the spent 30Ni_PS catalyst, in which spherical particles of 0.19 μm covered by nickel phyllosilicate layers were evidently observed. The average nickel particle size was slightly increased from 2.9 to 3.1 nm after the third cycle of reaction tests. It has been suggested that the fibrous nickel phyllosilicate structure can inhibit the growth of nickel particles and prevent the sintering/leaching of nickel particles during CO_2 methanation[16] and hydrogenation of maleic anhydride.[13] In contrast, the average Ni particle sizes on 20Ni_Imp increased from 29 to 35 nm, indicating that agglomeration of Ni particles on the silica support occurred under reaction conditions, and the number active sites were lower due to larger particle sizes. The atomic surface ratio of Ni^0/Si species decreased from 2.1 to 1.4 in the third run, suggesting a low Ni dispersion on the spent catalyst, as seen in Table S3. In addition, the nickel metal of the 20Ni_Imp catalyst tended to be leached during the cycles as a result of the weak interaction between Ni species and the silica support. These results led to a sharp decline in the catalytic performance for each run on the 20Ni_PS catalyst. The XPS spectra of the used 30Ni_PS catalyst confirmed the presence of nickel metal and nickel phyllosilicate domains after the third run. There was no obvious change in
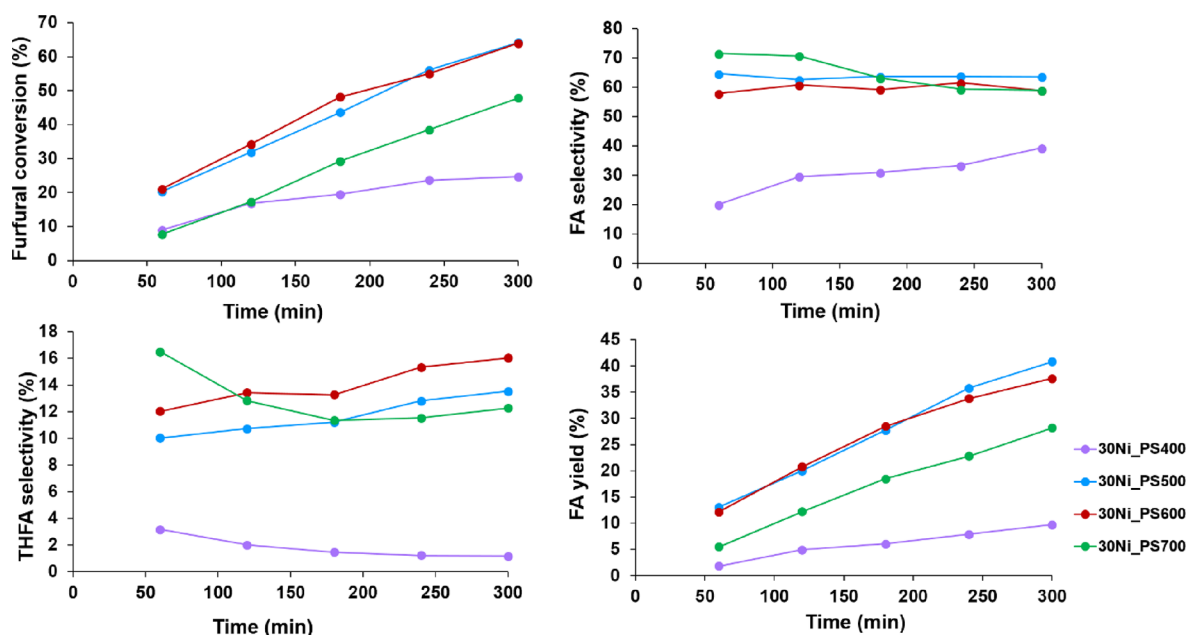
Figure 8. Hydrogenation of furfural to FA at different reduction temperatures over 30Ni_PS catalysts. Reaction conditions: 250 mg of catalyst, 3 mmol of furfural, 50 mL of methanol solvent, 0.4 mmol of dodecane, reaction temperature of 50 °C, 20 bar H_2 pressure, reaction time of 5 h.
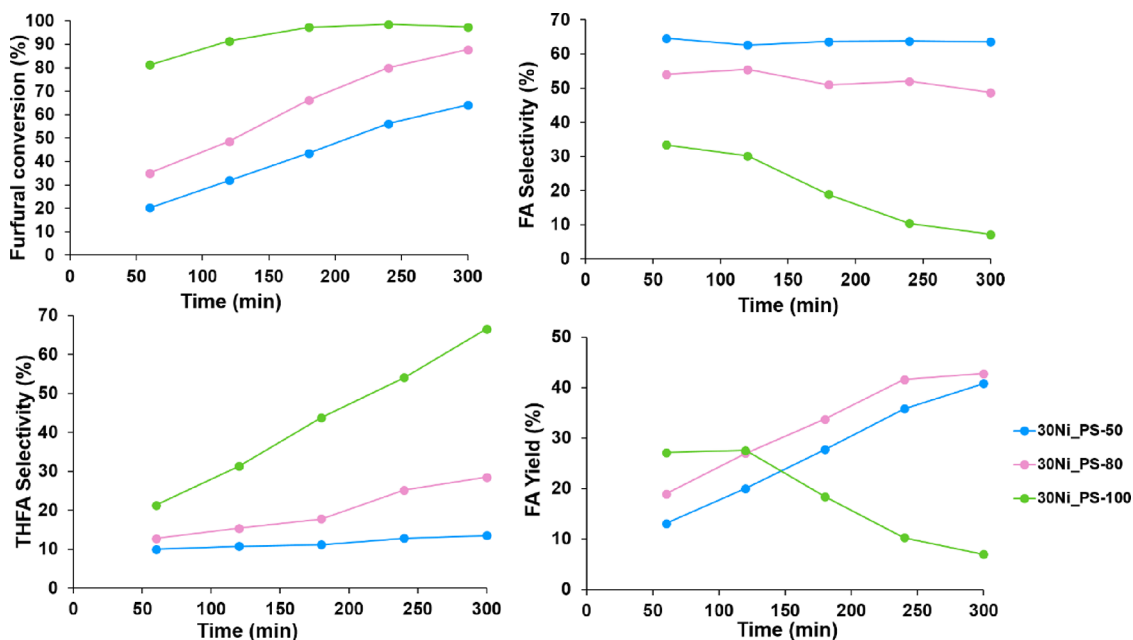

Figure 9. Hydrogenation of furfural to FA under different reaction temperatures over 30Ni_PS catalysts. Reaction conditions: 250 mg of catalyst, 3 mmol of furfural, 50 mL of methanol solvent, 0.4 mmol of dodecane, 20 bar H_2 pressure, reaction time of 5 h, and catalysts were reduced at 500 °C.

the XPS spectra before and after the reaction tests. The high stability of Ni_PS catalysts was ascribed to strong metal–support interaction and unique properties of Ni phyllosilicate where the unreduced Ni^{2+} could serve as a good support for the Ni^0 species, resulting in the active metallic nickel being highly dispersed with small size nickel particles.[31] Moreover, the atomic surface ratio of Ni^0/Si species increased from 0.36 to 0.57 on 30Ni_PS. Such results also suggest that nickel phyllosilicate species could be reduced into metallic Ni^0 during reaction on 30Ni_PS, which was still beneficial for reaction. The good recyclability of the Ni_PS catalysts was attributed to the strong interaction between nickel and the silica support and the high stability of the nickel phyllosilicate species that

can prevent agglomeration of Ni particles during reaction and re-reduction.[4,12,13]

Effects of Reduction Temperature and Reaction Temperature. The effects of reduction temperature and reaction temperature on the selective hydrogenation of furfural to FA were further investigated on the 30Ni_PS catalyst (Figure 8). Prior to the reactions, the 30Ni_PS catalyst was reduced under H_2 at 400−700 °C. The catalyst reduced at 400 °C yielded low furfural conversion. The highest furfural conversion and FA selectivity were obtained after 5 h of reaction time on the catalysts reduced at temperatures between 500 and 600 °C. Further increasing the reduction temperature to 700 °C led to a drop of furfural conversion, despite the

larger amount of metallic Ni^0 formed (from TPR and XPS results). Interestingly, the catalysts reduced at relatively high reduction temperatures (500, 600, and 700 °C) maintained their high selectivity to FA, varying from 60 to 70% during the 5 h reaction time with negligible amounts of THFA and undesired products.

The reduced catalysts were characterized by TEM, BET, and XPS analyses to correlate their characteristics with the catalytic performances. From the TEM results, the nickel phyllosilicate layers still existed on the surface of the 30Ni_PS catalysts. The average nickel particle sizes were slightly increased from 2.9 to 3.2 nm with increasing reduction temperature from 500 to 700 °C (Figure S5) but were still much smaller than the reduced 20Ni_Imp catalyst, as shown in Figure 2. Such results suggest that the reduction temperature has little effect on the particle size of metallic nickel being formed. The BET surface area, pore volume, and pore diameter of the reduced catalysts are presented in Table S4. There were no major differences in the structural properties of the reduced catalysts. They had similar average nickel particle sizes of ca. 3 nm with BET surface areas 236–257 m^2/g, pore volumes 0.11–0.13 cm^3/g, and pore diameters 4.3–4.4 nm. It confirms that the Ni_PS catalyst presented a high anti-sintering and prevented the agglomeration of nickel particles at high temperatures. However, as revealed by XPS results, the main peak, assigned to nickel phyllosilicate at around 857.6–859 eV, disappeared on the catalyst reduced at 700 °C and the peak corresponding to metallic Ni^0 species was observed at the binding energy 853.1 eV instead. The results suggest that a suitable proportion of metallic nickel and nickel phyllosilicate can enhance the catalytic performances of Ni_PS catalysts in the furfural hydrogenation to FA.

The influences of reaction temperature on the catalytic performances of 30Ni_PS on furfural conversion, FA selectivity, and FA yield are shown in Figure 9. Furfural conversion significantly increased with increasing reaction temperature and with increasing reaction time. The complete conversion of furfural (100%) was achieved at 100 °C. At 3 h reaction time, the furfural conversion was enhanced from 44 to 66% and reached 100% when the reaction temperature rose from 50 °C to 80 °C and 100 °C, respectively. The reaction temperature also had a significant impact on the product distribution. From the results, it is obviously seen that higher temperatures and longer reaction times promoted the deeper hydrogenation of the furan ring in furfural, resulting in higher selectivity toward THFA and lower FA selectivity. The optimum reaction temperature and reaction time to produce the highest yield of FA over the 30Ni-PS catalyst were 80 °C and 4 h reaction time, which gave 82% conversion and 42% yield of FA. A comparison of reaction conditions and catalytic performances with the other reported nickel-based catalysts in the selective furfural hydrogenation is shown in Table S5. From the table, the performances of catalysts prepared in this study in the form of nickel silicate were comparable to the other supported Ni/NiO catalysts. The mole ratios of furfural to nickel were varied among various studies. The complete conversion of furfural (100%) that was achieved over 30Ni_PS at 100 °C in this study may be due to the lower mole ratio of furfural to nickel than the others reported at 50–150 °C reaction temperature.

CONCLUSIONS

Spherical silica-supported nickel phyllosilicate catalysts were synthesized by one-step modified spherical silica synthesis at room temperature with nickel loadings of 2–30 wt % and evaluated in the liquid-phase selective hydrogenation of furfural to FA at 50 °C and 2 MPa H_2. The unique properties of nickel phyllosilicate were successfully obtained via a simple one-step synthesis strategy by an alternate addition of the nickel and silica sources during the spherical silica synthesis, yielding a high dispersion of small Ni particles (<3 nm) in the silica matrix, as well as nickel phyllosilicate species throughout the spherical particles, as revealed by TEM and XPS results. The strong interaction between nickel and the silica support and the unique structure of nickel phyllosilicate not only prevent Ni agglomeration during reaction and re-reduction but also facilitate furfural adsorption via the C=O bond through oxygen atoms, resulting in a higher FA yield and good recyclability. The nickel phyllosilicate catalysts were superior to the impregnated Ni on spherical silica, which suffered from agglomeration of nickel particles and a large portion of inactive NiO. Moreover, there appeared to be a synergistic effect due to the presence of both metallic nickel and nickel phyllosilicate that promoted FA formation under the reaction conditions used. The optimum reduction temperature, reaction temperature, and reaction time to produce the highest yield of FA (42%) over the nickel phyllosilicate catalyst with 30 wt % Ni were 500 °C, 80 °C, and 4 h reaction time, respectively. The attractive properties of Ni_PS catalysts show their great potential for furfural hydrogenation to FA under mild reaction conditions.

MATERIALS AND METHODS

Preparation of Spherical Silica. The spherical silica supports were prepared by using tetraethoxysilane (TEOS) as the silica source and hexadecyltrimethylammonium bromide (CTAB) as the structure-directing agent. The molar ratio of TEOS:CTAB: H_3:ethanol:H_2O was 1:0.3:11:58:114. First, a mixture of ethanol and distilled water was stirred at room temperature followed by the addition of aqueous ammonia. After that, CTAB was dissolved in the mixed solution under continuous stirring for 15 min, TEOS was added, and the mixed solution was further stirred for 2 h. Then, the obtained white precipitate was collected by filtration and washed with distilled water. Finally, the resulting powder was dried overnight at 110 °C and calcined at 550 °C for 6 h in air with a heating rate of 2 °C/min.

Loading of Nickel on Spherical Silica. Nickel nitrate hexahydrate was chosen as the nickel precursor and was incorporated into the spherical silica support by a one-step modified spherical silica synthesis method with different nickel loadings in the range of 2–30 wt %. The molar concentration of Ni precursor was in the range of 0.0049–0.0677 for 2–30 wt % nickel loading. After a solution of ethanol, aqueous ammonia, distilled water, and CTAB was continuously stirred for 15 min, the nickel precursor and TEOS were simultaneously loaded into the solution and further stirred for 2 h. The precipitate was separated by filtration, washed with distilled water, dried at 110 °C, and calcined at 550 °C for 6 h in air. The obtained catalysts are referred to as xNi_PS catalysts, where x indicates the percent nickel loading.

For comparison purposes, 20 wt % Ni on spherical silica was prepared by incipient wetness impregnation and is denoted as

the 20Ni_Imp catalyst. The spherical silica support was impregnated with an aqueous solution of nickel precursor followed by drying at 110 °C overnight and calcination in air at 550 °C for 6 h.

Catalytic Reactions. The obtained catalysts were used in the liquid phase hydrogenation of furfural in a 160 mL stainless steel Parr autoclave reactor with a Teflon liner. Prior to the reaction, the catalysts were reduced under H_2 flow at 500 °C for 3 h and then cooled to room temperature followed by passivation with $1\%O_2/N_2$ for 1 h. This passivation step was performed to protect and control the reduced catalysts from oxidation in air by creating an oxide layer over the metallic surface. The mole ratio of the furfural to nickel was 3.52. In a typical experiment, 3 mmol of furfural, 50 mL of methanol solvent, 0.25 g of the reduced/passivated catalysts, and 0.4 mmol of dodecane (internal standard) were charged into the autoclave. After that, it was purged with N_2 (300 psig, 2 min) five times and heated to a reaction temperature (50−100 °C) under N_2 to ensure a minimal reaction during heat up. When the reaction reached the target temperature, the autoclave reactor was purged with H_2 (500 psig, 2 min) five times and the reaction was carried out under 800 rpm stirring with 20 bar H_2 for 5 h. Samples were collected through a sampling port with a sample volume less than 300 μL for each sample (every 60 min) to minimize reaction volume losses. The liquid products were filtered and analyzed by a Shimadzu GC-2010 chromatograph using an auto sampler with a CP-Wax 58 FFAP CB column and a flame ionization detector. Furfural conversion, selectivity, and FA yield were calculated using dodecane as an internal standard. For the recyclability study, the catalysts were washed with methanol solvent several times and recycled for three cycles under the same reaction conditions.

Catalyst Characterization. X-ray diffraction (XRD) was conducted by using PaNalytical X'Pert Pro Alpha-1 diffractometer with Cu K_α radiation. XRD patterns of the calcined and reduced/passivated catalysts were measured in a range from 10 to 90° at room temperature. Nitrogen physisorption was carried out by a Micromeritics Tristar II 3020 at −196 °C. The samples (about 0.1 g) were pretreated at 180 °C for 10 h under vacuum prior to the nitrogen physisorption measurement. The average pore diameter and pore volume were determined using desorption isotherms by the BJH method. X-ray photoelectron spectroscopy (XPS) analysis was performed on the calcined and reduced/passivated catalysts in a Thermo K-Alpha spectrometer with a monochromatic Al Kα radiation source. H_2-temperature programmed reduction (H_2-TPR) and CO- pulse chemisorption were carried out on a Micromeritics AutoChem II 2920 equipped with a TCD to measure the reducibility and chemisorption uptake of the catalysts. For TPR experiments, the sample (0.03 g) was loaded on a bed of quartz wool in a quartz u-tube. First, the sample was pretreated under He flow at 200 °C for 1 h and was then cooled to 50 °C. The gas was switched to $10\%H_2/Ar$ flowing at 20 mL/min, and the sample was heated to 800 °C at a ramp rate of 10 °C/min. For CO-pulse chemisorption analysis, approximately 0.03 g of the catalyst was introduced into a quartz u-tube like the TPR experiment. Prior to the chemisorption, the catalyst was reduced under H_2 flow at 500 °C for 3 h and was then cooled to 400 °C with He flow for 30 min to remove weakly adsorbed species. After that, the sample was cooled to 40 °C followed by CO-pulse chemisorption testing. Doses of 10%CO/He were passed over the reduced catalyst until saturation was obtained,

as analyzed in the TCD. Finally, He was passed over the sample for 60 min. Scanning transmission electron microscopy (STEM) images and EDS element mapping were obtained on a Hitachi HD 2700. TEM samples were dispersed in ethanol, and then the suspension was dropped on a TEM grid.

■ ASSOCIATED CONTENT

ⓢ Supporting Information

The Supporting Information is available free of charge at https://pubs.acs.org/doi/10.1021/acsomega.2c03590.

> N_2 adsorption−desorption isotherm; carbon balance; physical properties, TEM images and Ni 2p XPS spectra at different reduction temperatures; TEM images, Ni 2p XPS spectra, and Ni species proportion of the freshly reduced and spent catalysts; and review of reaction condition, TOF value, and mole ratio of furfural to nickel in furfural hydrogenation (PDF)

■ AUTHOR INFORMATION

Corresponding Authors

Christopher W. Jones − *School of Chemical & Biomolecular Engineering, Georgia Institute of Technology, Atlanta, Georgia 30332, United States*; Email: cjones@chbe.gatech.edu

Joongjai Panpranot − *Center of Excellence on Catalysis and Catalytic Reaction Engineering, Department of Chemical Engineering, Faculty of Engineering and Bio-Circular-Green-Economy Technology & Engineering Center, BCGeTEC, Department of Chemical Engineering, Faculty of Engineering, Chulalongkorn University, Bangkok 10330, Thailand; Department of Chemical & Petroleum Engineering, Faculty of Engineering, Technology and Built Environment, UCSI University, 56000 Kuala Lumpur, Malaysia;* ⓞ orcid.org/0000-0002-0398-5912; Email: joongjai.p@chula.ac.th

Authors

Sasithorn Kuhaudomlap − *Center of Excellence on Catalysis and Catalytic Reaction Engineering, Department of Chemical Engineering, Faculty of Engineering, Chulalongkorn University, Bangkok 10330, Thailand; School of Chemical & Biomolecular Engineering, Georgia Institute of Technology, Atlanta, Georgia 30332, United States*

Okorn Mekasuwandumrong − *Department of Chemical Engineering, Faculty of Engineering and Industrial Technology, Silpakorn University, Nakhon Pathom 73000, Thailand*

Piyasan Praserthdam − *Center of Excellence on Catalysis and Catalytic Reaction Engineering, Department of Chemical Engineering, Faculty of Engineering, Chulalongkorn University, Bangkok 10330, Thailand;* ⓞ orcid.org/0000-0001-8021-2115

Kiat Moon Lee − *Department of Chemical & Petroleum Engineering, Faculty of Engineering, Technology and Built Environment, UCSI University, 56000 Kuala Lumpur, Malaysia;* ⓞ orcid.org/0000-0003-1126-9657

Complete contact information is available at:
https://pubs.acs.org/10.1021/acsomega.2c03590

Notes

The authors declare no competing financial interest.

■ ACKNOWLEDGMENTS

■ REFERENCES

(1) Li, H.; Chen, Y.; Liu, S.; Liu, Q. Enhancement of hydrothermal synthesis of FDU-12-derived nickel phyllosilicate using double accelerators of ammonium fluoride and urea for CO_2 methanation. *J. CO2 Util.* **2021**, *52*, 101677.

(2) Mallesham, B.; Sudarsanam, P.; Venkata Shiva Reddy, B.; Govinda Rao, B.; Reddy, B. M. Nanostructured Nickel/Silica Catalysts for Continuous Flow Conversion of Levulinic Acid to γ-Valerolactone. *ACS Omega* **2018**, *3*, 16839−16849.

(3) Wu, X.; Xu, L.; Chen, M.; Lv, C.; Wen, X.; Cui, Y.; Wu, C. E.; Yang, B.; Miao, Z.; Hu, X. Recent Progresses in the Design and Fabrication of Highly Efficient Ni-Based Catalysts With Advanced Catalytic Activity and Enhanced Anti-coke Performance Toward CO_2 Reforming of Methane. *Front. Chem.* **2020**, *8*, 581923.

(4) Zhang, T.; Liu, Q. Lanthanum-Modified MCF-Derived Nickel Phyllosilicate Catalyst for Enhanced CO_2 Methanation: A Comprehensive Study. *ACS Appl. Mater. Interfaces* **2020**, *12*, 19587−19600.

(5) Zhang, Y.; Chen, Y.; Liu, Q. Green synthesis of MCM-41 derived from renewable biomass and construction of VOx-Modified nickel phyllosilicate catalyst for CO_2 methanation. *Int. J. Hydrogen Energy* **2021**, *46*, 32003−32016.

(6) Zhang, T.; Liu, Q. Perovskite LaNiO3 Nanocrystals inside Mesostructured Cellular Foam Silica: High Catalytic Activity and Stability for CO2 Methanation. *Energy Technol.* **2020**, *8*, 1901164.

(7) Manikandan, M.; Venugopal, A. K.; Prabu, K.; Jha, R. K.; Thirumalaiswamy, R. Role of surface synergistic effect on the performance of Ni-based hydrotalcite catalyst for highly efficient hydrogenation of furfural. *J. Mol. Catal. A: Chem.* **2016**, *417*, 153−162.

(8) Ingale, P.; Guan, C.; Kraehnert, R.; Naumann d'Alnoncourt, R.; Thomas, A.; Rosowski, F. Design of an active and stable catalyst for dry reforming of methane via molecular layer deposition. *Catal. Today* **2021**, *362*, 47−54.

(9) Wang, X.; Zhu, S.; Wang, S.; Wang, J.; Fan, W.; Lv, Y. Ni nanoparticles entrapped in nickel phyllosilicate for selective hydrogenation of guaiacol to 2-methoxycyclohexanol. *Appl. Catal., A* **2018**, *568*, 231−241.

(10) Yang, H.; Zhang, Y.; Liu, Q. Highly Efficient Ni-Phyllosilicate Catalyst with Surface and Interface Confinement for CO_2 and CO Methanation. *Ind. Eng. Chem. Res.* **2021**, *60*, 6981−6992.

(11) Li, C.-C.; Hsieh, C.-H.; Lin, Y.-C. Ni/SiO2 catalysts derived from carbothermal reduction of nickel phyllosilicate in the hydrogenation of levulinic acid to γ-valerolactone: The efficacy of nitrogen decoration. *Mol. Catal.* **2022**, 111720.

(12) Du, H.; Ma, X.; Jiang, M.; Yan, P.; Zhao, Y.; Conrad Zhang, Z. Efficient Ni/SiO2 catalyst derived from nickel phyllosilicate for xylose hydrogenation to xylitol. *Catal. Today* **2021**, *365*, 265−273.

(13) Tan, J.; Xia, X.; Cui, J.; Yan, W.; Jiang, Z.; Zhao, Y. Efficient Tuning of Surface Nickel Species of the Ni-Phyllosilicate Catalyst for the Hydrogenation of Maleic Anhydride. *J. Phys. Chem. A* **2019**, *123*, 9779−9787.

(14) Wang, M.; Qian, X.; Xie, L.; Fang, H.; Ye, L.; Duan, X.; Yuan, Y. Synthesis of a Ni Phyllosilicate with Controlled Morphology for Deep Hydrogenation of Polycyclic Aromatic Hydrocarbons. *ACS Sustainable Chem. Eng.* **2018**, *7*, 1989−1997.

(15) Wei, Y.; Horlyck, J.; Song, M.; Scott, J.; Amal, R.; Cao, Q. Inducing Ni phyllosilicate formation over a carbon fiber support as a catalyst for the CO_2 reforming of methane. *Appl. Catal., A* **2020**, *592*, 117418.

(16) Dong, H.; Liu, Q. Three-Dimensional Networked Ni-Phyllosilicate Catalyst for CO_2 Methanation: Achieving High Dispersion and Enhanced Stability at High Ni Loadings. *ACS Sustainable Chem. Eng.* **2020**, *8*, 6753−6766.

(17) Sivaiah, M. V.; Petit, S.; Beaufort, M. F.; Eyidi, D.; Barrault, J.; Batiot-Dupeyrat, C.; Valange, S. Nickel based catalysts derived from hydrothermally synthesized 1:1 and 2:1 phyllosilicates as precursors for carbon dioxide reforming of methane. *Microporous Mesoporous Mater.* **2011**, *140*, 69−80.

(18) Chen, Y.; Bi, W.; Chen, L.; Liu, Q. Urea-assisted synthesis towards a renewable rice husk silica-derived Ni-phyllosilicate catalyst for CO_2 methanation. *Int. J. Hydrogen Energy* **2021**, *46*, 27567−27575.

(19) Wang, Y. W.; Zhang, Y. J.; Wang, K. J.; Tan, L. M.; Chen, S. Y. Preparation of Ni/SiO2 by ammonia evaporation method for synthesis of 2-MTHF from 2-MF hydrogenation. *J. Fuel Chem. Technol.* **2021**, *49*, 97−103.

(20) Yang, F.; Wang, H.; Han, J.; Ge, Q.; Zhu, X. Enhanced selective deoxygenation of m-cresol to toluene on Ni/SiO2 catalysts derived from nickel phyllosilicate. *Catal. Today* **2019**, *330*, 149−156.

(21) Ye, R.-P.; Gong, W.; Sun, Z.; Sheng, Q.; Shi, X.; Wang, T.; Yao, Y.; Razink, J. J.; Lin, L.; Zhou, Z.; Adidharma, H.; Tang, J.; Fan, M.; Yao, Y.-G. Enhanced stability of Ni/SiO2 catalyst for CO_2 methanation: Derived from nickel phyllosilicate with strong metal-support interactions. *Energy* **2019**, *188*, 116059.

(22) Ciotonea, C.; Hammi, N.; Dhainaut, J.; Marinova, M.; Ungureanu, A.; El Kadib, A.; Michon, C.; Royer, S. Phyllosilicate-derived Nickel-cobalt Bimetallic Nanoparticles for the Catalytic Hydrogenation of Imines, Oximes and N-heteroarenes. *ChemCatChem* **2020**, *12*, 4652−4663.

(23) Alencar, J. M.; Oliveira, F. J. V. E.; Airoldi, C.; Silva Filho, E. C. Organophilic nickel phyllosilicate for reactive blue dye removal. *Chem. Eng. J.* **2014**, *236*, 332−340.

(24) Chen, Y.; Zhang, T.; Liu, Q. One-pot or two-pot synthesis? Using a more facile and efficient method to synthesize Ni-phyllosilicate catalyst derived from 3D-SBA-15. *Int. J. Hydrogen Energy* **2021**, *46*, 30373−30381.

(25) Zhang, T.; Tian, Z.; Liu, Q. Three-dimensional flower-like nickel phyllosilicates for CO_2 methanation: enhanced catalytic activity and high stability. *Sustainable Energy Fuels* **2020**, *4*, 3438−3449.

(26) Chen, Y.; Liu, Q. Synthesis and Regeneration of Ni-Phyllosilicate Catalysts Using a Versatile Double-Accelerator Method: A Comprehensive Study. *ACS Catal.* **2021**, *11*, 12570−12584.

(27) Liu, H.; Zou, X.; Wang, X.; Lu, X.; Ding, W. Effect of CeO2 addition on Ni/Al2O3 catalysts for methanation of carbon dioxide with hydrogen. *J. Nat. Gas Chem.* **2012**, *21*, 703−707.

(28) Zhao, B.; Chen, Z.; Chen, Y.; Ma, X. Syngas methanation over Ni/SiO2 catalyst prepared by ammonia-assisted impregnation. *Int. J. Hydrogen Energy* **2017**, *42*, 27073−27083.

(29) Yang, M.; Wu, H.; Wu, H.; Huang, C.; Weng, W.; Chen, M.; Wan, H. Preparation and characterization of a highly dispersed and stable Ni catalyst with a microporous nanosilica support. *RSC Adv.* **2016**, *6*, 81237−81244.

(30) Zhang, Y.; Liu, Q. Nickel phyllosilicate derived Ni/SiO2 catalysts for CO_2 methanation: Identifying effect of silanol group concentration. *J. CO2 Util.* **2021**, *50*, 101587.

(31) Kong, X.; Zhu, Y.; Zheng, H.; Li, X.; Zhu, Y.; Li, Y.-W. Ni Nanoparticles Inlaid Nickel Phyllosilicate as a Metal−Acid Bifunctional Catalyst for Low-Temperature Hydrogenolysis Reactions. *ACS Catal.* **2015**, *5*, 5914−5920.

(32) Moogi, S.; Lee, I.-G.; Park, J.-Y. Effect of La2O3 and CeO2 loadings on formation of nickel-phyllosilicate precursor during preparation of Ni/SBA-15 for hydrogen-rich gas production from ethanol steam reforming. *Int. J. Hydrogen Energy* **2019**, *44*, 29537−29546.

(33) Wang, C.; Tian, Y.; Wu, R.; Li, H.; Yao, B.; Zhao, Y.; Xiao, T. Bimetallic Synergy Effects of Phyllosilicate-Derived NiCu@SiO2

Catalysts for 1,4-Butynediol Direct Hydrogenation to 1,4-Butanediol. *ChemCatChem* **2019**, *11*, 4777−4787.

(34) Meng, X.; Yang, Y.; Chen, L.; Xu, M.; Zhang, X.; Wei, M. A Control over Hydrogenation Selectivity of Furfural via Tuning Exposed Facet of Ni Catalysts. *ACS Catal.* **2019**, *9*, 4226−4235.

(35) Bell, J. M.; Kubler, D. G.; Sartwell, P.; Zepp, R. G. Acetal Formation for Ketones and Aromatic Aldehydes with Methanol1. *J. Org. Chem.* **1965**, *30*, 4284−4292.

(36) Taylor, M. J.; Durndell, L. J.; Isaacs, M. A.; Parlett, C. M. A.; Wilson, K.; Lee, A. F.; Kyriakou, G. Highly selective hydrogenation of furfural over supported Pt nanoparticles under mild conditions. *Appl. Catal., B* **2016**, *180*, 580−585.

(37) Şebin, M. E.; Akmaz, S.; Koc, S. N. Hydrogenation of furfural to furfuryl alcohol over efficient sol-gel nickel-copper/zirconia catalyst. *J. Chem. Sci.* **2020**, *132*, 157.

(38) Liu, L.; Lou, H.; Chen, M. Selective hydrogenation of furfural to tetrahydrofurfuryl alcohol over Ni/CNTs and bimetallic Cu Ni/CNTs catalysts. *Int. J. Hydrogen Energy* **2016**, *41*, 14721−14731.

(39) Sang, S.; Wang, Y.; Zhu, W.; Xiao, G. Selective hydrogenation of furfuryl alcohol to tetrahydrofurfuryl alcohol over Ni/γ-Al2O3 catalysts. *Res. Chem. Intermed.* **2017**, *43*, 1179−1195.

(40) MacIntosh, K. L.; Beaumont, S. K. Nickel-Catalysed Vapour-Phase Hydrogenation of Furfural, Insights into Reactivity and Deactivation. *Top. Catal.* **2020**, *63*, 1446−1462.

(41) Xu, J.; Cui, Q.; Xue, T.; Guan, Y.; Wu, P. Total Hydrogenation of Furfural under Mild Conditions over a Durable Ni/TiO(2)-SiO(2) Catalyst with Amorphous TiO(2) Species. *ACS Omega* **2020**, *5*, 30257−30266.

(42) Halilu, A.; Ali, T. H.; Atta, A. Y.; Sudarsanam, P.; Bhargava, S. K.; Abd Hamid, S. B. Highly Selective Hydrogenation of Biomass-Derived Furfural into Furfuryl Alcohol Using a Novel Magnetic Nanoparticles Catalyst. *Energy Fuels* **2016**, *30*, 2216−2226.

(43) Gong, W.; Chen, C.; Zhang, H.; Zhang, Y.; Zhang, Y.; Wang, G.; Zhao, H. Highly selective liquid-phase hydrogenation of furfural over N-doped carbon supported metallic nickel catalyst under mild conditions. *Mol. Catal.* **2017**, *429*, 51−59.

(44) Gong, W.; Chen, C.; Wang, H.; Fan, R.; Zhang, H.; Wang, G.; Zhao, H. Sulfonate group modified Ni catalyst for highly efficient liquid-phase selective hydrogenation of bio-derived furfural. *Chin. Chem. Lett.* **2018**, *29*, 1617−1620.

(45) Wu, J.; Liu, C.; Zhu, Y.; Song, X.; Wen, C.; Zhang, X.; Wang, C.; Ma, L. Understanding the geometric and electronic factors of PtNi bimetallic surfaces for efficient and selective catalytic hydrogenation of biomass-derived oxygenates. *J. Energy Chem.* **2021**, *60*, 16−24.

(46) Fan, Y.; Zhuang, C.; Li, S.; Wang, Y.; Zou, X.; Liu, X.; Huang, W.; Zhu, G. Efficient single-atom Ni for catalytic transfer hydrogenation of furfural to furfuryl alcohol. *J. Mater. Chem. A* **2021**, *9*, 1110−1118.

(47) Wu, J.; Yan, X.; Wang, W.; Jin, M.; Xie, Y.; Wang, C. Highly Dispersed CoNi Alloy Embedded in N-doped Graphitic Carbon for Catalytic Transfer Hydrogenation of Biomass-derived Furfural. *Chem. - Asian J.* **2021**, *16*, 3194−3201.